Journal of Cancer Research and Clinical Oncology (2025) 151:112
https://doi.org/10.1007/s00432-025-06159-0

RESEARCH

# Developing and validating a prognostic disulfidptosis-related signature for glioblastoma: predicting radioresistance and synergestic effect with immunotherapy

**Chen Chen[1,2,3] · Peixin Tan[3] · Wenqing Feng[1,2,3] · Yuan Lei[3] · Shushu Hu[1,2,3] · Dehuan Xie[3] · Yantan Liu[3] · Chen Ren[1,2,3] · Shasha Du[1,2,3]**

Received: 3 December 2024 / Accepted: 5 March 2025 / Published online: 18 March 2025


## Abstract

**Background** Programmed cell death (PCD) modulated radioresistance is one of the predominant causes of treatment failure in glioblastoma (GBM). Disulfidptosis, a newly discovered form of PCD, plays a crucial role in GBM progression. However, the association among disulfidptosis, radiosensitivity and radiotherapy (RT) in GBM remain unclear.

**Methods** We systematically analyzed disulfidptosis-related genes in 1075 GBM patients and constructed a disulfidptosis-related gene signature (DRS). Correlations among the DRS, patient prognosis and immune microenvironment were fully explored. The effects of DRS and EFEMP2 on radiotherapy efficacy were investigated via single cell sequencing analysis and validated via in vitro and in vivo experiments.

**Results** The DRS was identified as a robust and independent prognostic biomarker for GBM by multivariate Cox regression analysis, receiver operating characteristic (ROC) curve analysis and decision curve analysis (DCA) in multiple cohorts. High DRS is characterized by radioresistance, and EFEMP2 was proven to be the key gene involved in this process by single cell sequencing analysis, CCK-8 assay and a clonogenic survival assay. In high-DRS patients, the cancer-immunity cycle is attenuated because the antitumor cytotoxicity of CD8+ T cells is inhibited by immune checkpoints. Preclinically, the overexpression of EFEMP2 induced radioresistance and enhancing the efficacy of programmed cell death ligand-1 (PD-L1) blockade in GL261-bearing mice. The combination of irradiation and anti-PD-L1 therapy had a synergistic effect on GBM murine models in which EFEMP2 was overexpressed.

**Conclusion** Our study bioinformatically and experimentally reveals the molecular landscape of disulfidptosis in GBM, develops a predictive signature for predicting prognosis as well as radioresistance, and provides a synergistic treatment that combines radiotherapy with immunotherapy for radioresistant GBM patients with high DRS or EFEMP2 expression.

**Keywords** Disulfidptosis · Tumor microenvironment · Glioblastoma · Radiotherapy · Immunotherapy

Chen Chen and Peixin Tan contributed equally to this work.

✉ Chen Ren
renchen@smu.edu.cn

✉ Shasha Du
dushasha8557@smu.edu.cn

[1] Southern Medical University, Guangzhou 510515, China

[2] Guangdong Provincial People's Hospital (Guangdong Academy of Medical Sciences), Southern Medical University, Guangzhou, China

[3] Department of Radiation Oncology, Guangdong Provincial People's Hospital, Southern Medical University, Guangzhou, China

## Abbreviations

| | |
|---|---|
| DRGs | Disulfidptosis-related genes |
| DRS | Disulfidptosis-related gene signature |
| GBM | Glioblastoma |
| TPM | Transcripts per million |
| NMF | Nonnegative matrix factorization |
| PCA | Principal component analysis |
| TOM | Topological overlap matrix |
| NTP | Nearest template prediction |
| GSEA | Gene set enrichment analysis |
| PPI | Protein-protein interaction |
| TIDE | Tumor immune dysfunction and exclusion |
| AUC | Area under the curve |
| ROC | Receiver operating characteristic |
| DCA | Decision curve analysis |

| | |
|---|---|
| PN | Proneural |
| CL | Classical |
| MES | Mesenchymal |
| CNV | Copy number variation |
| WGCNA | Weighted correlation network analysis |
| RR | Radioresistant |
| CR | Chemoresistant. |
| DC | Dendritic cell |
| GSC | Glioma stem cell |
| M1 | M1-macrophatge |
| M2 | M2-macrophage |
| RSI | Radiosensitivity index |
| PD | Progressive disease |
| SD | Stable disease |
| PR | Partial response |
| CR | Complete response |
| IR | Irradiation |
| ICB | Immune checkpoint blockade |

## Background

Glioblastoma (GBM), accounting for 50% of central nervous system malignancies, is the most aggressive, and fatal primary intracranial malignant tumor in adults with an annual increase in frequency (Stupp et al. 2017). Despite combination therapy including surgical resection, radiotherapy (RT), and chemotherapy (CT), the prognosis for glioblastoma patients remains poor, with a median survival of 14-16 months and a five-year survival rate of less than 10% (Stupp et al. 2017). GBM tends to develop resistance during radiotherapy, which can lead to therapeutic failure (Johannessen et al. 2013). Immunotherapy is considered as a promising approach for reversing radioresistance. Preclinically, immune checkpoint blockade (ICB) effectively promoted radiotherapy efficacy (Zeng et al. 2013; Kim et al. 2017). However, human clinical trials have failed to mirror the success of the combination of immunotherapy and radiotherapy. The results from the CheckMate 498 (NCT02617589) and CheckMate 548 (NCT02667587) studies demonstrated that immune checkpoint inhibitors (ICIs) did not prolong the overall survival (OS) of patients with newly diagnosed GBM (Sampson, et al. 2016; Lim et al. 2022). However, in the phase I of CheckMate 143 (NCT02017717) study, the progression-free survival (PFS) of GBM patients treated with ICI+RT+CT differed according to the $O^6$-methylguanine DNA methyltransferase (MGMT) promoter status (Reardon et al. 2020). Additionally, ICI treatment extended the median survival time for recurrent GBM patients with methylated MGMT in phase III of the CheckMate 143 study compared with bevacizumab. These results indicate that the combination of radiotherapy and immunotherapy might not be a universal therapeutic option for GBM, and a better stratification is needed to harness the potential of radioimmunotherapy.

Programmed cell death (PCD) in tumor cells can be induced by radiation, facilitating antitumor immunity by promoting tumor antigen presentation and activating immune cells (Lang et al. 2019). Disulfidptosis, a newly discovered form of programmed cell death, is driven by the aberrant accumulation of intracellular disulfides (Liu et al. 2023). SLC7A11-dependent collapse of disulfide bonds in the actin cytoskeleton and F-actin, which directly triggers cell death was found in $SLC7A11^{high}$ tumor cells under glucose starvation. By performing CRISPR screens, genes required for disulfidptosis and genes whose deactivation promotes disulfidptosis were identified as disulfidptosis-related genes (DRGs) (Wang et al. 2023a; Chen et al. 2023). Recent studies revealed the prognostic and therapeutic value of disulfidptosis in GBM (Yang et al. 2024; Zhou et al. 2024). However, the relationship between disulfidptosis and radiosensitivity is neglected. Hence, exploring the influence of disulfidptosis on glioblastoma treatments provides new insights into the radioresistance of GBM and even improves the efficacy of radiotherapy.

In this study, we thoroughly explored the impact of the disulfidptosis-related genes in 1075 GBM patients from three cohorts. Disulfidptosis was correlated with patient prognosis and clinicopathological features. A disulfidptosis-related prognostic signature (DRS) was subsequently generated and found to be highly correlated with poor prognosis, radioresistance, and immunosuppression. Single-cell analysis and in vitro and in vivo experiments revealed that high DRS manipulated the radioresistance phenotype of GBM and that the overexpression of EFEMP2 from DRS reduced the radiosensitivity of GBM cells. In addition, we confirmed the improved immunotherapeutic efficacy and a synergistic therapeutic effect of immunotherapy and radiotherapy in high-DRS GL261-bearing C57BL/6 mice. Taken together, our study provides a new perspective on disulfidptosis and develops a possible synergistic radioimmunotherapeutic strategy.

## Methods

### Data acquisition

Transcriptional data and corresponding clinical data of glioblastoma patients were obtained from public databases. Microarray data were downloaded from the GlioVis platform, including datasets from TCGA (n = 528), Rembrandt (n = 219), Gravendeel (n = 159), and Ducray (n = 52) (Bowman et al. 2016). RNA-seq data were acquired from the UCSC database for TCGA-GBM (n = 175) and the CGGA database for CGGA-GBM (n = 388) (Goldman

et al. 2020). All of the count data were then converted to transcripts per million (TPM) format and further log2 transformed. The CGGA-325 dataset and CGGA-693 dataset were merged into the CGGA dataset for further analyses. Batch effects from nonbiological technical biases were corrected via the "ComBat" algorithm of the "sva" package (Leek et al. 2012; Zhao et al. 2021). Other cohorts with expression data were collected from the GEO database, including transcriptome profiles of a radioresistant GBM cell line (GSE207002), a temozolomide-resistant GBM cell line (GSE151680), and immunotherapy-treated melanoma cohorts from GSE100797 (n = 25) and GSE91061 (n = 51) (Lauss et al. 2017; Riaz et al. 2017). The single-cell dataset of 28 GBM patients (GSE131928) and its metadata were obtained from the single-cell portal database (Neftel et al. 2019).

### Unsupervised clustering analysis

The nonnegative matrix factorization (NMF) algorithm executed in the "NMF" package was used to identify molecular clustering by factorizing the matrix and running iterations. On the basis of the nonnegative expression matrix of DRGs, consensus clustering was deciphered with the following criteria in the NMF package: possible factorization ranks ranged from 2 to 10. The cophenetic coefficient was employed to determine the optimal rank and the optimal factorization rank was the value at which the cophenetic correlation coefficient started decreasing. Principal component analysis (PCA) was then performed to validate the distinction of the clusters with R package "stats".

### Weighted gene coexpression network analysis and differential gene analysis

Weighted gene coexpression network analysis (WGCNA) aims to explore and reveal the correlations between gene modules and phenotypes (Langfelder and Horvath 2008). The hub genes of the disulfidptosis-related clusters were identified via the WGCNA package. First, after the outlier samples were filtered out, a gene coexpression network was produced based on the top 5000 genes and further transformed into a scale-free network by selecting an appropriate soft threshold b. Second, the topological overlap matrix (TOM) which represents the overlap of network neighbors, and the 1-TOM, which describes gene dissimilarity were generated via the weighted adjacency matrix. Finally, various colored gene modules were identified via the dynamic tree algorithm. Based on the relationships between the module eigenvalue and phenotypes, the two modules with the highest correlations were filtered, and the hub genes were acquired for subsequent analysis. By using the R package "limma", we obtained DEGs between the two clusters with screening conditions of $|\log(FC)| > 1$ and adjusted $P < 0.05$.

### Nearest template prediction validation

Nearest template prediction (NTP) is an approach to evaluate class prediction confidence for a single patient and was carried out with the R package "CMScaller" (Hoshida 2010). The input for NTP consisted of a normalized expression data and a signature gene list constructed by intersecting hub genes, identified through WGCNA with differentially expressed genes (DEGs).

### Functional enrichment analysis

Functional enrichment was used to better understand the carcinogenesis of different DRG patterns. Gene set enrichment analysis (GSEA) and single-sample gene set enrichment analysis (ssGSEA) were run with the "ClusterProfiler" package to identify the different pathways. Gene sets were retrieved from the Molecular Signature Database (MSigDB) (Liberzon et al. 2015).

### Construction and validation of the disulfidptosis-related gene signature

Microarray data from the TCGA-GBM cohort was used to identify the disulfidptosis-related clusters and construct a disulfidptosis-related gene signature (DRS). We first present a protein-protein interaction (PPI) network with DEGs in the STRING database and calculate the betweenness score of each gene with Ctyo-Hubba in Cytoscape software (Szklarczyk et al. 2019). We selected 30 subtype-related genes for Lasso Cox regression analysis via the R package "glmnet". The calculation formula is as follows:

$$\mathrm{DRS} = \sum(Coefi * Exp)$$

In this formula, Coefi indicates the risk coefficient, and Exp indicates the expression level. Patients from each cohort were categorized into a high DRS group and a low DRS group according to the median DRS. Survival analyses were then conducted to compare the prognostic differences between the two groups.

### Establishment of a disulfidptosis-related nomogram system

A nomogram was drawn via the "rms" package. Each patient was given a predicted score on the basis of their age and DRS score, which was used for accurately predicting 0.5-, 1- and 1.5-year survival accurately. The prognostic value of the

nomogram was then evaluated via calibration analysis and receiver operating characteristic curve (ROC) curve analysis.

## Tumor microenvironment assessment and single-cell RNA-seq data analysis

Cell infiltration, as well as the ESTIMATE score, was calculated with IOBR, an R package that performs a comprehensive analysis of the tumor microenvironment and features for immuno-oncology (Zeng et al. 2021). The Seurat package was utilized to process data for further dimension reduction and cell clustering analysis. PCA linear dimensional reduction and clustering visualization were performed via the "RunPCA" function and the "RunUMAP" function of Seurat. The function "AverageExpression" was used to generate a normalized expression data for each patient, based on which the DRS of each patient was calculated. Patients in the single-cell dataset were divided into two DRS groups according to the median DRS. CellChat analysis was performed with the "CellChat" package.

## The evaluation of clinical treatment

The tumor immune dysfunction and exclusion (TIDE) algorithm and subclass mapping (Submap) were used to predict the clinical response to immune checkpoint blockade (Fu et al. 2020; Hoshida et al. 2007). The submap algorithm was used to assess the similarity of gene expression between the two DRS groups identified and the melanoma patients who received immunotherapy (Lu et al. 2019). Expression data were preprocessed according to the guidelines provided on the respective websites. Formal analyses were then performed using the TIDE platform (http://tide.dfci.harvard.edu/) and the GenePattern platform (https://www.genepattern.org/#gsc.tab=0).

## Cell culture and transfection of glioma cell lines

Human glioma cell lines (LN229, U87, and T98G) and Human Glial Cell Line (Heb) were purchased from Pricella, China. and the American Type Culture Collection (ATCC). GL261 (murine glioblastoma) cells were obtained from Guangzhou KOFA Biotechnology Company. The cells were cultured in DMEM medium with 10% fetal bovine serum. All the cell lines were maintained in a humidified incubator with 5% $CO_2$, at 37 °C. The EFEMP2 overexpression lentivirus (Beijing Tsingke Biotech Co., Ltd.) is transfected into LN229 and GL261 cells. Following this, puromycin (2 μg/mL) was added to facilitate the screening of successfully infected cell colonies.

## Cell viability assay

LN229 cells stably overexpressing EFEMP2 were subjected to exposure to a 6-MV X-ray beam at doses as indicated, and cultured for 24, 48 and 72 hours. The culture medium was replaced with 100 μL of fresh medium containing 10% Cell Counting Kit-8 reagent (FDbio Science) for a subsequent two-hour incubation period in a humidified incubator under standard conditions. Cell viability was assessed according to the absorbance at 450 nm measured by a Bio-Rad microplate reader, following the protocol provided by the manufacturer.

## Clonogenic survival assays

LN229 cells were seeded in triplicate into twelve-well plates and irradiated at different doses as indicated. Once visible colonies had formed after a period of 7–10 days of incubation, the cells were washed with phosphate-buffered saline (PBS) and then fixed with 4% paraformaldehyde for a period of 15 minutes. 0.5% crystal violet (Macklin) was subsequently used to stain the colonies for 30 min. The surviving fraction was calculated by counting colonies comprising more than 50 cells.

## Western blot analysis

Cells were washed three times with ice-cold PBS and subsequently lysed in RIPA buffer (FD009, Fdbio Science) on ice for 30 minutes. Then, the lysate was centrifuged at 12,000 × g for 15 minutes at 4 °C. A BCA protein assay kit (Thermo) was used to assess protein concentration. Proteins (20 μg per sample) were separated on a 12.5% SDS-PAGE gel and transferred to polyvinylidene difluoride (PVDF) membranes (ISEQ00010, Merck Millipore). The membranes were blocked with 5% skim milk in TBST for 60 minutes at room temperature, then incubated overnight at 4 °C with primary antibodies targeted EFEMP2 (ab125073, Abcam) and GAPDH (ET1601-4, HUABIO). After this, the membranes were washed and treated with an HRP-conjugated secondary antibody for 1 hour at room temperature.

## Real time PCR

Total RNA was extracted with TRIzol Reagent (Invitrogen). Reverse transcription was carried out using the Reverse Transcription System Kit (TaKaRa). cDNA expression levels were then quantified using SYBR Green (TaKaRa) and qRT-PCR, with β-actin as the internal reference. The sequences of primers used were EFEMP2-F: 5′-AAGAGCCCGACAGCTACAC-3′, EFEMP2-R: 5′-AGGGATGGTCAGACACTCGTT-3′;

β-actin-F: 5′-TGGCACCCAGCACAATGAA-3′, β-actin-R: 5′-CTAAGTCATAGTCCGCCTAGAAGCA-3′.

### In vivo experiments

Six-to-eight-week-old C57BL/6 mice (Guangdong Medical Laboratory Animal Center) were anesthetized and immobilized on a stereotactic frame. A total of $2\times10^5$ GL261 cells (EFEMP2-Fluc-Puro) in 5 μl Hank's balanced salt solution (HBSS) was injected at a depth of 4 mm, a lateral position of 2.0 mm from bregma, and a ventral position of 2.0 mm from the dura in the right hemisphere. mice were randomly assigned to treatment groups based on tumor burden assessed via luciferase imaging on day 5 after implantation. Tumor-bearing mice received either whole brain irradiation (10 Gy) or intraperitoneal administration of anti-PD1 (BioXCell, BE0146-100MG, 10 mg/kg). Luciferase imaging was used to monitor tumor burden of mice regularly. At the endpoint, the mice were euthanized using $CO_2$ inhalation followed by Pentobarbitone administration (50 mg/kg, iv), and the brains were harvested for further analysis.

### Statistical analysis

GraphPad Prism 8 and R statistical software (v4.2.3) were used to perform all the statistical tests and generate all the figures. Kaplan-Meier survival analysis was conducted using the R packages 'survival' and 'survminer.' Univariate and multivariate Cox regression analyses were performed with the 'survival' package. Time-dependent areas under curve (AUC) values were calculated using the 'timeROC' package, while ROC curves were generated with the 'survivalROC' package. Calibration analysis and decision curve analysis (DCA) were conducted with the 'rms' and 'ggDCA' package. The Wilcoxon rank-sum test was used to assess differences in DRS values, gene expression, and immune infiltration scores across various comparison groups, including high- and low-DRS groups, as well as radioresistant, chemo-resistant, and normal GBM cell lines. Fisher's exact test was used to assess the differences in the distribution of various clinicopathological characteristics or therapeutic responses between the high- and low-DRS groups. All the statistical tests were two-sided. $P < 0.05$ was considered statistically significant. Significant symbols are ordered as follows: **** < 0.001 < *** < 0.001 < ** < 0.01 < * < 0.05.

## Results

### Identification and validation of disulfidptosis-related clusters in glioblastoma

The status of seven programmed cell death (PCD) processes was evaluated in the pancancer dataset via ssGSEA based on well-established gene sets obtained from the literature and MSigDB database (Supplementary Table S1) (Liu et al. 2023; Zhang, et al. 2024). We found that the disulfidptosis score in GBM was the highest among all cancers, whereas the scores of other types of PCD were relatively low, suggesting disulfidptosis may be distinctive to GBM (Fig. 1A). Thus, we conducted NMF analysis based on the disulfidptosis related genes (DRGs) in the TCGA cohort (Supplementary Table S1). According to the consensus heatmap and silhouette value, GBM patients were finely classified into two clusters, which were referred to as C1 and C2 (Supplementary Fig. S1A). PCA confirmed that the disulfidptosis-related clusters were distinct from each other (Supplementary Fig. S1B). Nearest template prediction (NTP) analysis was applied to identifiy disulfidptosis clusters of GBM patients in the CGGA and Gravendeel datasets (Supplementary Fig. S1C). Survival analysis suggested that C1 patients had a worse prognosis than C2 patients did in all three datasets (Fig. 1B, Supplementary Fig. S1D, E). We then compared the clinical and molecular pathological features between the two clusters. In C1, higher proportions of classical and mesenchymal subtypes, and a greater tendency toward IDH mutation were observed (Fig. 1C and Supplementary Fig. S1F, G). We also noted that the proportions of secondary GBM and proneural subtypes were greater in C2 (Fig. 1C and Supplementary Fig. S1F). These findings indicate that the transcript levels of DRGs are correlated with the malignancy of GBM, which prompted the question of whether the survival of GBM patients could be predicted through DRG expression.

### Construction and validation of the disulfidptosis-related gene signature

We first utilized WGCNA to acquire gene modules associated with the disulfidptosis clusters. During WGCNA, we acquired 12 coexpression modules by setting the beta at 6 when the nonscale $R^2$ was 0.8. The module–trait relationships revealed that the blue module was correlated with C1, and the red module was related to C2 (Fig. 2A). We also obtained differentially expressed genes ($|\log2FC|\geq1$ and P value < 0.05) from the two clusters (Fig. 2B). By intersecting cluster markers and module

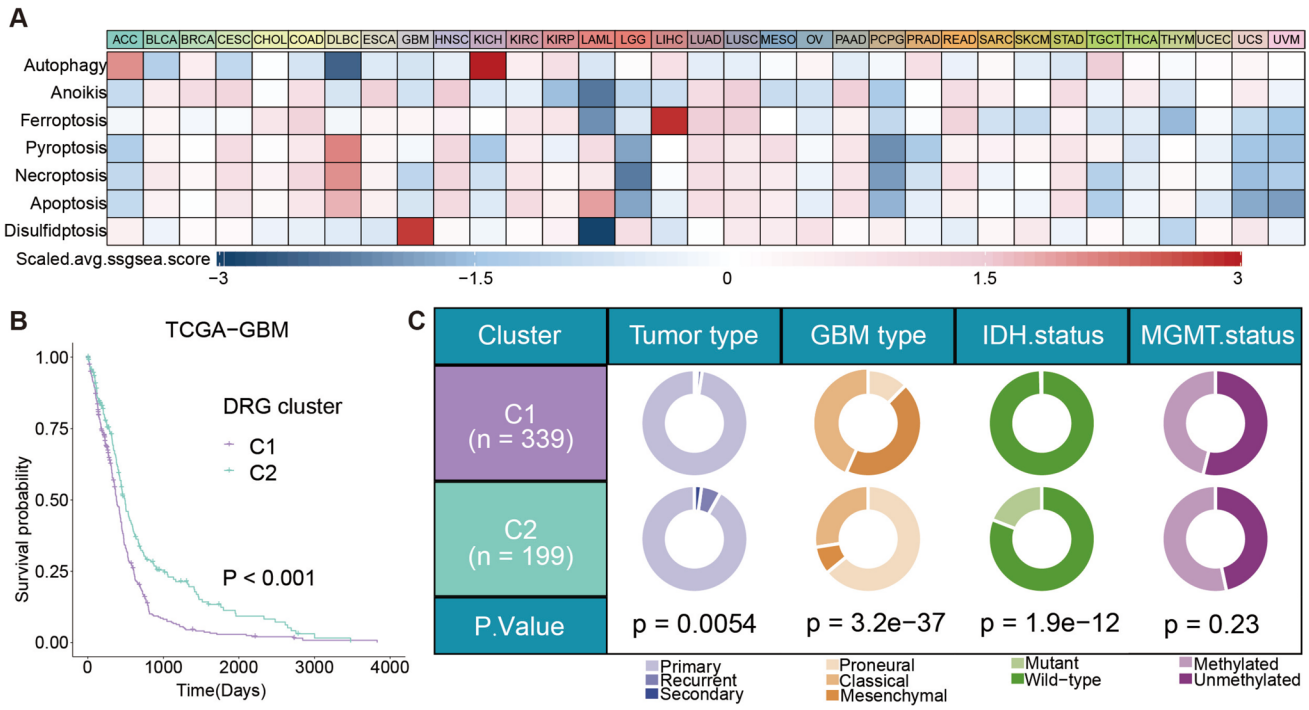


**Fig. 1** Identification of disulfidptosis-related clusters. **A** Scaled averaged ssGSEA scores of seven PCD in pan-cancer. **B** Kaplan–Meier analysis (log-rank test) of the disulfidptosis-related clusters in TCGA cohort. **C** Clinical pathological features of the disulfidptosis-related clusters in pie charts (Fisher's test)

genes, we obtained characteristic genes, which were narrowed down to 30 on the basis of the betweenness scores calculated via protein-protein interaction (PPI) network analysis (Fig. 2C, D and Supplementary Table S2). Next, the Lasso-Cox regression was conducted with characteristic genes to construct a prognostic model (disulfidptosis-related gene signature, DRS) (Supplementary Fig. S2A and Supplementary Table S3). GBM patients were then separated into a high-DRS group and a low-DRS group for further analyses according to the median score. The Sankey plots showed that the majority of C1 had a relatively high DRS (Fig. 2E and Supplementary Fig. S2B).

The high-DRS group had a better prognosis than the low-DRS group did ($P < 0.001$) (Fig. 2F and Supplementary Fig. S2C, H). The receiver operating characteristic (ROC) curve and the decision curve analysis (DCA) showed that DRS outperformed other published signatures in predictive performance (Fig. 2G, H and Supplementary Fig. S2D, E, I, J) (Zhang et al. 2023; Wang et al. 2023b; Sun and Liu 2024; Fan et al. 2022; Zhang et al. 2023). Additionally, the univariate and multivariate Cox regression analyses revealed that the DRS, alone with age, was an independent prognostic indicator (Figure 2I and Supplementary Fig. S2F, K).

However, we recognize that there is still room for improvement in the predictive power of DRS. Thus, we constructed a nomogram to further enhance its performance (Fig. 2J). Subsequent calibration analysis, ROC curve analysis, and DCA demonstrated a further improvement in the ability of the nomogram to predict 1-year survival compared to DRS alone, suggesting that integrating DRS with other clinical variables enhances predictive performance and provides a potential strategy for its clinical application. (Fig. 2K–M and Supplementary Fig. S2G, L).

## Evaluation of the relationship between DRS and therapeutic response in GBM

Treatment resistance is believed to account for the poor prognosis of GBM patients (Johannessen et al. 2013). We compared the therapeutic response of the DRS groups in the Ducray cohort. The response rate to radiotherapy was lower in the high-DRS group (55.6% vs. 63.2%), while there was no difference in the chemotherapeutic response rate between the two groups (50.0% vs. 50.0%) (Fig. 3A). In addition, compared with that in untreated GBM cells, DRS was increased in radioresistant GBM cells but not in temozolomide-resistant GBM cells (Fig. 3B). For patients who underwent radiotherapy or even radiotherapy alone in all three cohorts, patients with high DRSs had shorter survival (Fig. 3C, D). However, for the patients who did not receive radiotherapy, no prognostic difference was observed between the two groups in any of the three cohorts (Fig. 3E). These

findings indicated that the DRS was positively correlated with the radioresistance of GBM patients.

## Single-cell analysis and validation in vitro identified EFEMP2 as the key gene of DRS associating with GBM cellular radioresistance

The causes of radioresistance can be attributed to in two factors: intrinsic resistance in tumor cells and microenvironment-related resistance (Xia et al. 2018; Yin et al. 2020). To reveal the mechanism of radiosensitivity heterogeneity in the DRS groups, we acquired a single cell dataset, GSE131928, and reannotated immune cells with canonical cell markers (Fig. 4A). Nonmalignant cells were annotated as macrophages (marked with CD163, F13A1, IL-10, MRC1, IL-1B, PTGS2, CCL4, and GPNMB), microglials (marked with TMEM119, and P2RY12), neutrophils (marked with S100A9 and S100A8), $CD4^+$ T-cells (marked with CD3E, CD3D, CD4, and CTLA4), $CD8^+$ T-cells (marked with CD3E, CD3D, CD8A, and CD8B) and oligodendrocyte (marked with OLIG1 and OLIG2) (Szulzewsky et al. 2015; Zeiner et al. 2019; You et al. 2023; Hu et al. 2022; Rajendran et al. 2023; Zhang et al. 2018). Higher proportions of nonmalignant cells were found in the high DRS group (Fig. 4B).

The malignant cells from the high-DRS group had lower ssGSEA scores for radiosensitivity (Fig. 4C). Subsequently, we carried out cell trajectory analysis and found that the malignant cells from the high-DRS group were mainly located mainly at the beginning of the cell trajectory (Fig. 4D). The radiosensitivity index is a gene signature revealing the radioresistance of tumor cells (Eschrich et al. 2009). Consequently, we calculated the RSI for each malignant cell and discovered that high-RSI cells also resided at the start of the trajectory, which was in accordance with the notion of the low radiosensitivity of glioma stem cells (GSCs) (Fig. 4D). These results demonstrated that the DRS was negatively correlated with radiosensitivity. Additionally, the transcriptome levels of mesenchymal glioma stem cell (MES-GSC) markers (e.g., CD44 and YKL40) were greater in the high-DRS group than in the low-DRS group and decreased in pseudotime. Conversely, the expression levels of proneural GSC markers (e.g., CD133 and OLIG2) elevated in the low DRS group and increased by the pseudotime (Supplementary Fig. S3A).

Among the five DRS genes, EFEMP2 and TIMP1 were the prominent genes expressed in malignant cells (Fig. 4E and Supplementary Fig. S3B). However, qPCR showed that only EFEPM2 was highly expressed in all glioma cell lines, suggesting that EFEMP2 may be the key gene regulating the radiosensitivity of GBM cells (Fig. 4F; Supplementary Fig. S3C). On the other hand, EFEMP2 had the highest weight in the DRS (Supplementary Table S3). Based on these findings, we chose EFEMP2 for subsequent analysis. The overexpression of EFEMP2 significantly promoted the tolerance of GBM cells to ionizing radiation and their ability to proliferate (Fig. 4G, H; Supplementary Fig. S3D; Supplementary Fig. S4A, B). These results indicate that DRS reflects the cellular radiosensitivity of GBM.

## Exploration of the correlation of DRS with the immunosuppressive microenvironment of GBM

GSEA was applied to investigate the mechanisms underlying the differences in prognosis and radiosensitivity between the DRS groups. Several immune related biological processes were enriched in the high DRS group (Fig. 5A; Supplementary Fig. S5A, B). The TIMER algorithm was used to evaluate the infiltration of immune cells in the GBM cohort, which revealed that the fractions of macrophages, dendritic cells, neutrophils, CD4+ T cells and CD8+ T cells increased in the high-DRS group (Fig. 5B; Supplementary Fig. S5C, D). Similar results were observed in the GSE131928 (Fig. 4B). These findings illustrated that the high DRS group might be characterized by a relatively active immune microenvironment and good prognosis, which contradicts our previous results. To elucidate the possible mechanisms of this paradoxical phenomenon, we conducted tracking tumor immunophenotype (TIP) analysis. TIP analysis revealed that the release and presentation of cancer cell antigens (Steps 1 and 2) and the trafficking and infiltration of immune cells (Steps 4 and 5) were significantly activated in the high DRS group (Fig. 5C; Supplementary Fig. S5E). Interestingly, highly activated early steps failed to enhance the cytotoxicity of T cells (Step 7) in the high DRS group (Fig. 5C; Supplementary Fig. S5E). Downregulated expression of cytotoxic makers was observed in $CD8^+$ T-cells in the high DRS group (Fig. 5D). Immune escape is orchestrated by immune checkpoints, attenuating of cytotoxicity (Aktar et al. 2022). In the three GBM cohorts, high expression of immune checkpoints was detected in the high DRS group (Fig. 5E; Supplementary Fig. S5F). Further analysis revealed that increased expression of PD-1 on CD8+ T-cells and PD-L1 on malignant cells in the high DRS group (Fig. 5F). These results indicated that the antitumor immunity of the high DRS group was hindered by immune checkpoints at the execution stage.

## Immunotherapy reversed the radioresistance phenotype of GBM cells overexpressing EFEMP2 in vivo

Given that the antitumor immunity of radioresistant GBM with a high DRS is diminished by immune checkpoints, immunotherapy might be an optimal treatment. By using the TIDE and submap algorithms, the immunotherapy response

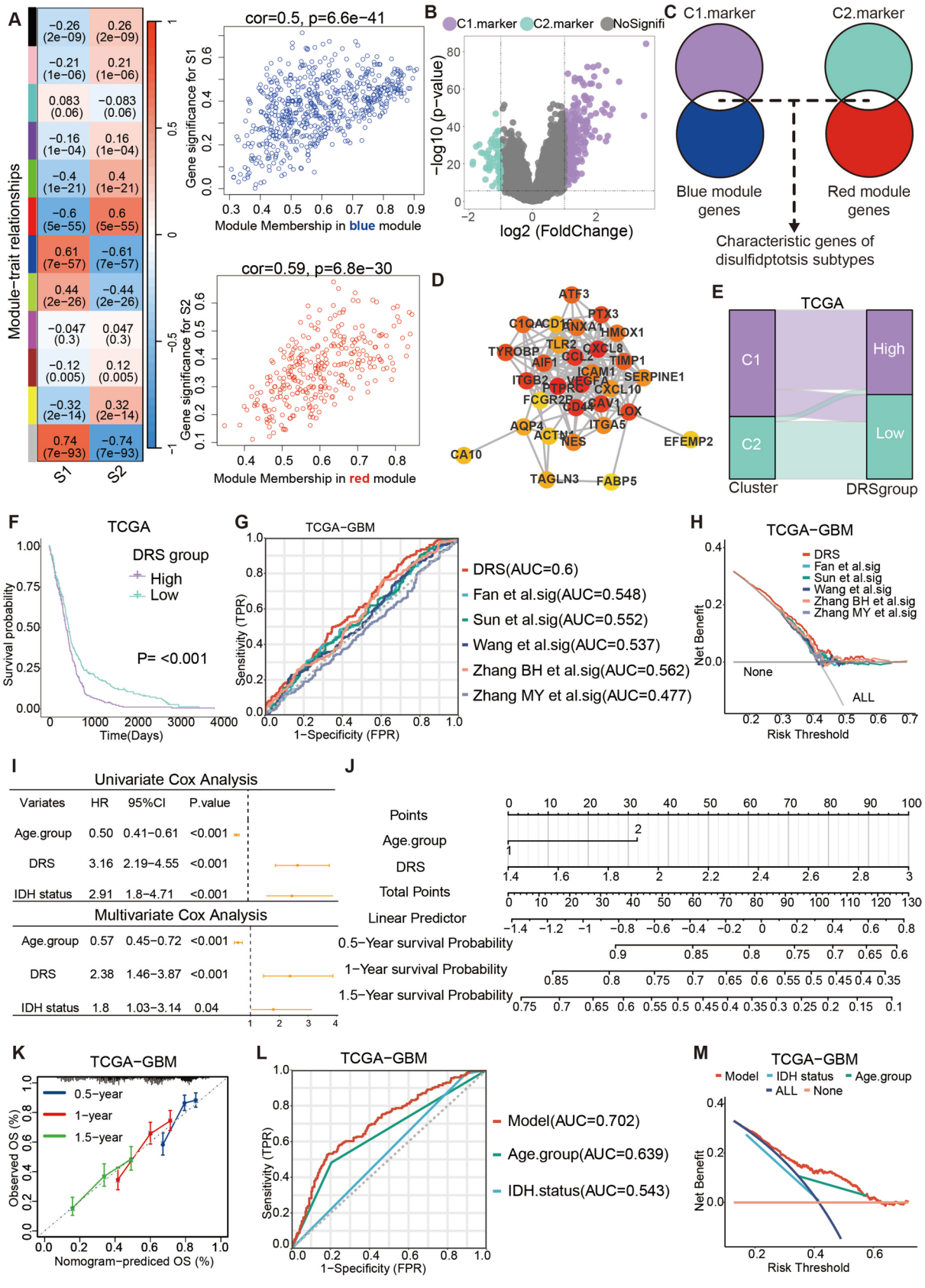
A
Module−trait relationships
S1
S2
cor=0.5, p=6.6e−41
Gene significance for S1
Module Membership in blue module
cor=0.59, p=6.8e−30
Gene significance for S2
Module Membership in red module
B
C1.marker
C2.marker
NoSignifi
−log10 (p−value)
log2 (FoldChange)
C
C1.marker
C2.marker
Blue module genes
Red module genes
Characteristic genes of disulfidptotsis subtypes
D
ATF3
PTX3
C1QAC
ANXA1
HMOX1
TYROBP
TLR2
CXCL8
AIF1
CCL2
TIMP1
ICAM1
ITGB2
SERPINE1
VEGFA
PTPRC
CXCL10
FCGR2B
CAV1
LOX
AQP4
ITGA5
ACTN1
NES
EFEMP2
CA10
TAGLN3
FABP5
E
TCGA
C1
C2
High
Low
Cluster
DRSgroup
F
TCGA
DRS group
High
Low
P= <0.001
Survival probability
Time(Days)
G
TCGA−GBM
Sensitivity (TPR)
1−Specificity (FPR)
DRS(AUC=0.6)
Fan et al.sig(AUC=0.548)
Sun et al.sig(AUC=0.552)
Wang et al.sig(AUC=0.537)
Zhang BH et al.sig(AUC=0.562)
Zhang MY et al.sig(AUC=0.477)
H
TCGA−GBM
DRS
Fan et al.sig
Sun et al.sig
Wang et al.sig
Zhang BH et al.sig
Zhang MY et al.sig
Net Benefit
None
ALL
Risk Threshold
I
Univariate Cox Analysis
Variates HR 95%CI P.value
Age.group 0.50 0.41−0.61 <0.001
DRS 3.16 2.19−4.55 <0.001
IDH status 2.91 1.8−4.71 <0.001
Multivariate Cox Analysis
Age.group 0.57 0.45−0.72 <0.001
DRS 2.38 1.46−3.87 <0.001
IDH status 1.8 1.03−3.14 0.04
J
Points
Age.group
DRS
Total Points
Linear Predictor
0.5−Year survival Probability
1−Year survival Probability
1.5−Year survival Probability
K
TCGA−GBM
0.5−year
1−year
1.5−year
Observed OS (%)
Nomogram−prediced OS (%)
L
TCGA−GBM
Sensitivity (TPR)
1−Specificity (FPR)
Model(AUC=0.702)
Age.group(AUC=0.639)
IDH.status(AUC=0.543)
M
TCGA−GBM
Model
IDH status
Age.group
ALL
None
Net Benefit
Risk Threshold

◂**Fig. 2** Construction of the disulfidptosis-related gene signature. **A** Identification of modular genes associated with disulfidptosis related clusters by WGCNA. **B** Volcano plot of differential expressed genes of the two clusters. **C** Schematic illustration of acquisition of the characteristic genes of the clusters. **D** PPI network of the top 30 characteristic genes ordered by their betweenness. **E** Sankey plot demonstrated the correspondence between the disulfidptosis-related clusters and scores. **F** Kaplan–Meier analysis of high-DRS and low-DRS groups in the TCGA cohort. **G**, **H** ROC curve and DCA curve depicting the performance of the DRS and other published gene signatures predicting 1-year OS. **I** Univariate and multivariate Cox regression of OS in the TCGA cohort. **J** The nomogram to predict 0.5-, 1.0-, and 1.5-year OS. **K** Calibration curve eliciting the performance of the nomogram in the TCGA cohort. **L**, **M** ROC curve and DCA curve depicting the performance of the DRS and other well-established biomarkers of GBM predicting 1-year OS

of patients from the TCGA and CGGA cohorts was estimated, suggesting that the high DRS group was sensitive to immune checkpoint blockade ($P < 0.05$) (Fig. 6A, C). On the other hand, there were more immunotherapy responders (PR/CR) in the high DRS group than in the low DRS group in the GSE91061 and GSE100797 cohorts (Fig. 6B). To determine whether high DRS GBM could benefit from immunotherapy, GL261/GL261-OE-EFEMP2 cells were implanted into C57BL/6J mice, which were then treated with an anti-PD-1 antibody alone, radiation alone, or their combination ($n = 6$) (Fig. 6D). The upregulated expression of EFEMP2 triggered radioresistance in the GL261-bearing mouse model (Fig. 6E, F). Additionally, high expression of EFEMP2 sensitized GBM to immune checkpoint blockade (Fig. 6E, F). Notably, the combination of radiation and an anti-PD-1 antibody exhibited a synergistic efficacy in mice overexpressing EFEMPE2, which was not observed in a mouse model without this combination (Fig. 6F). These findings revealed that increased expression of EFEMP2 was responsible for GBM resistance to radiation but sensitivity to ICB, which could inform the development of a synergistic radioimmunotherapeutic strategy.

## Discussion

Exploration of disulfiptosis can provide new knowledge for the radioresistance of GBM. Here, we elucidate the role of disulfidptosis in glioblastoma genesis, offering information about disulfidptosis-related genes, the tumor microenvironment, radiotherapy, and immunotherapy. Our study can be pursued with the ultimate goal of optimizing glioblastoma management.

Disulfidptosis has been explored as a marker of GBM associated with prognosis and the TME (Yang et al. 2024; Zhou et al. 2024). Although estimation analysis in silico estimation analysis revealed that DRGs are correlated with the response to seldomly used treatments and immunotherapy for GBM, we still have limited knowledge of the clinical significance of disulfidptosis in GBM because we have not explored whether the expression of DRGs affects the efficacy of standard regimens and verified the immunotherapeutic relevance of models in experimental or clinical cohorts (Yang et al. 2024; Zhou et al. 2024). In this study, we comprehensively analyzed disulfidptosis at the transcriptome level and developed a gene signature named DRS, which could serve as a solid biomarker for the development of more effective therapeutic strategies for GBM. The DRS exhibits superior prognostic predictive ability for GBM patients compared to existing gene signatures, as validated in large sample sizes across multiple cohorts. Additionally, the DRS can serve as a valuable tool for predicting radiosensitivity. Single-cell analysis revealed that a high DRS was associated with the expression of MES-GSC markers. Glioma stem cells (GSCs) are one of the main reasons for cellular radioresistance. Among the two subtypes of GSCs, the MES-GSCs represent a relatively malignant subtype of GBM cells that are renowned for resistance to conventional therapy (Wang et al. 2021; Bao et al. 2006). In addition, the DRS was positively correlated with the RSI, a quantitative tool of tumor cellular radioresistance. Previous studies have shown that the RSI has limitations in predicting patient prognosis and response to radiation (Grimes 2022). Our research demonstrated that DRS reflects radioresistance not only at the individual level but also at the cellular level.

EFEMP2 was identified as the key gene in DRS with exclusive expression on tumor cells and a correlation with radioresistance. The role of EFEMP2 in tumorigenesis varies considerably across different types of cancer. EFEMP2 serves as a protective factor in bladder, breast and lung cancers (Zhou et al. 2019; Kang et al. 2019; Song et al. 2020). Moreover, EFEMP2 was able to enhance the invasion of ovarian and cervical cancers and glioma (Shen et al. 2023; Li et al. 2022). However, the role of EFEMP2 in tumorigenesis varies significantly across different cancer types. In bladder and lung cancers, EFEMP2 has been reported to suppress EMT via the Wnt/β-catenin signaling pathway, whereas in osteosarcoma, EFEMP2 has been shown to promote EMT through the STEAP2/PI3K/AKT/mTOR pathway (Zhou et al. 2019; Song et al. 2020; Zhang et al. 2022).

Although the precise mechanisms remain unclear, multiple studies have confirmed the tumor-promoting role of EFEMP2 in glioblastoma (Wang et al. 2015; Huang et al. 2020). As early as 2010, Verhaak et al. proposed that GBM can be classified into three molecular subtypes: mesenchymal (MES), classical (CL), and proneural (PN) (Verhaak et al. 2010). Among them, the mesenchymal subtype (MES) is considered the most aggressive and therapy-resistant form of GBM (Yu et al. 2024). Isrel et al. suggested that the

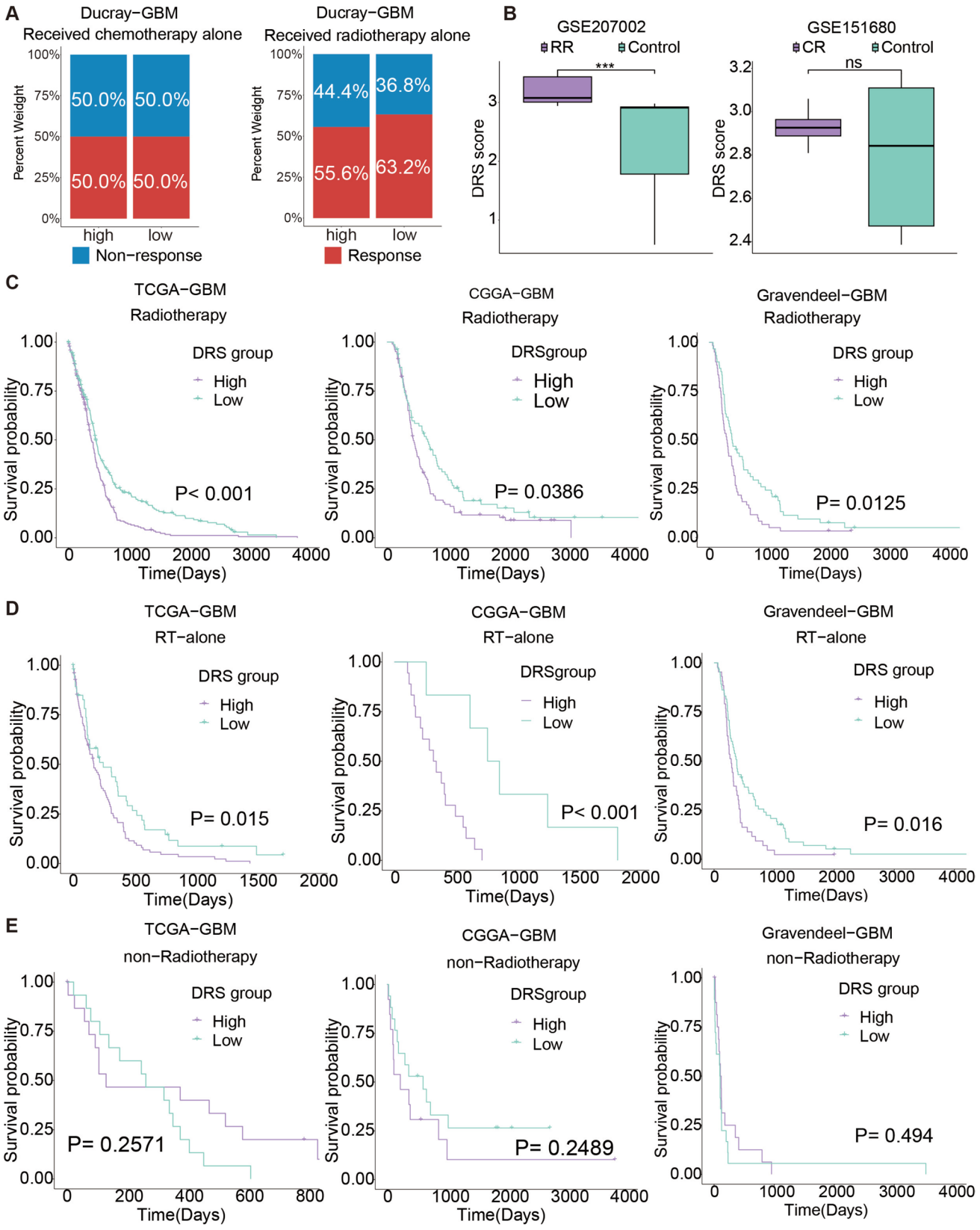


**Fig. 3** The correlation between the DRS and radioresistance. **A** The therapeutic response rate of GBM patients with different DRS score in the Ducray cohort. **B** The DRS score among therapeutic response at cell level. **C–E** Kaplan-Meier survival analysis of DRS in subgroups in three cohorts (log-rank test). *RT* radiotherapy, *RR* radioresistant, *CR* chemoresistant

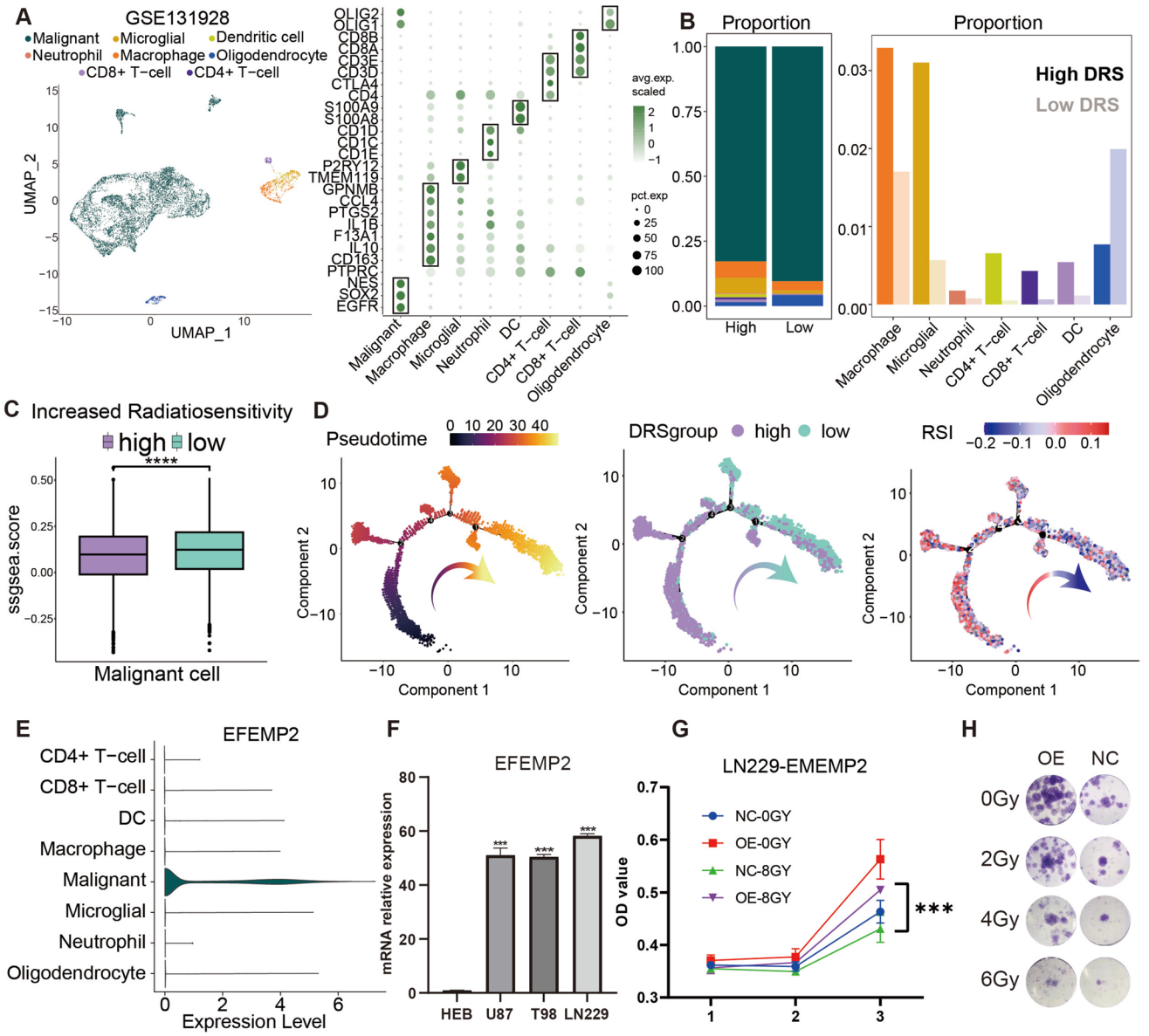


**Fig. 4** The DRS was correlated with cellular radioresistance. **A** UMAP plot of tumor-infiltrating cells in GSE131928 (left) and dot plot showing the signature gene expression of cell types (right). **B** The proportion of cells that contributed to each cell type by the DRS groups. Color annotations match those of the UMAP plot. **C** Difference in ssGSEA scores of 'HP_INCREASED_SENSITIVITY_TO_IONIZING_RADIATION' pathway between malignant cells from each DRS group. **D** Pseudotime (left), the DRS group (middle) and radiosensitivity index (right) visualized on the cell trajectory plot of malignant cells. **E** Violin plots showing expression of EFEMP2 among cell types. **F** The transcriptional differences of EFEMP2 between GBM cells and normal brain cells. **G** The evaluation of radioresistance of EFEMP2-OE GBM cells by CCK8 assay. **H** The evaluation of radioresistance of EFEMP2-OE GBM cells utilizing clonogenic survival assay

mesenchymal phenotype of GBM may arise from an EMT-like biological process (Iser et al. 2017).

In our analysis of the TCGA cohort, we observed that high EFEMP2 expression is significantly associated with the 'glioblastoma mesenchymal', 'epithelial-mesenchymal transition' gene sets (Additional File 2). High EFEMP2 GBM also enriched in 'TGFB_EMT_UP' and 'HIF1_TFPATHWAY' terms, which were considered as trigger signals of EMT process. What's more, High EFEMP2 GBM enriched in 'BOQUEST_STEM_CELL_UP', which is consistent with our single-cell RNA sequencing analysis results. These findings indicate a strong link between EFEMP2 expression and mesenchymal-like cell states in GBM, which collectively suggest that EFEMP2 may promote the mesenchymal phenotype of GBM via EMT. However, the functionally

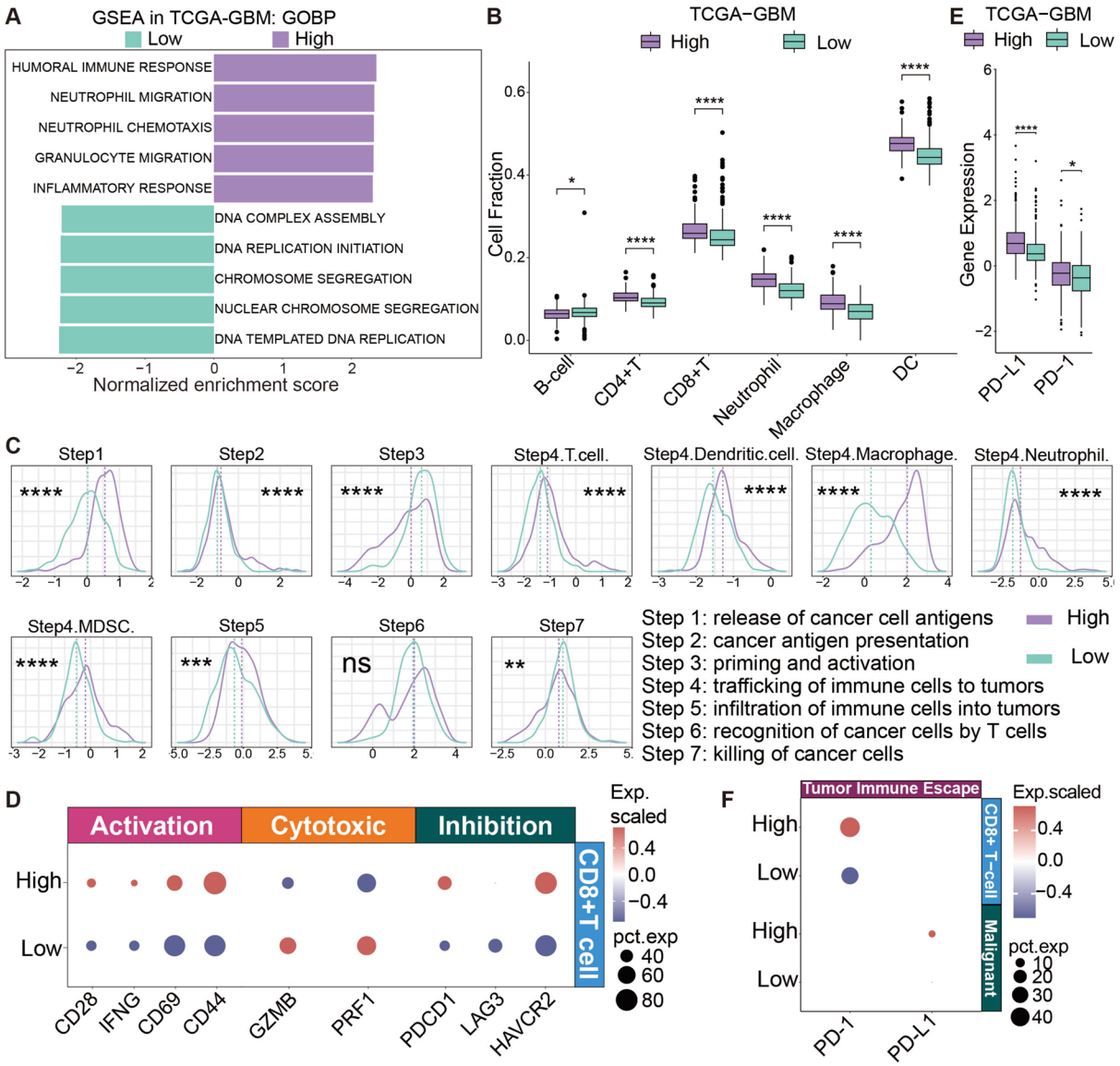


**Fig. 5** The DRS was associated with immunosuppression. **A** GSEA results of the DRS groups. **B** Differential analysis of infiltration of immune cell estimated by TIMER algorithm between the DRS groups. **C** Tracking tumor immunophenotype analysis of the DRS groups in the CGGA cohort. **D** Differential expression analysis showing genes related to T cell activation, cytotoxic and inhibition in $CD8^+$ T cell. **E** Differential expression of immune check points in the TCGA cohort. **F** Differential expression analysis of genes associated with tumor immune escape in $CD8^+$ T cells and malignant cells

characterizing this process and the signaling pathways involved required further investigations.

In addition to directly killing tumor cells, radiotherapy can activate antitumor immunity to diminish tumor lesions (Wu et al. 2014). Our findings suggest that even though a high DRS represents increased tumor antigen presentation and increased infiltration of immune cells, it is still correlated with poor prognosis and radioresistance. This paradox was attributeis attributed to the low cytotoxicity of T cells triggered by the overexpression of PD-1/PD-L1. The overexpression of immune checkpoints was observed after RT, resulting in immunosuppression and radioresistance (Pineda et al. 2019; Deng et al. 2014). Thus, ICB was applied to ameliorate radioresistance by offsetting such immunosuppression. Regrettably, ICB did not yield significant results in clinical trials, which can be explained by our study. A previous study revealed that the expression levels of PD-1/PD-L1 modulated the efficacy of ICB (Sun et al. 2023). We detected differences in the expression of PD-1/PD-L1 between the DRS groups, suggesting the possible selective efficacy of immunotherapy for GBM. In tumor immune analyses, we

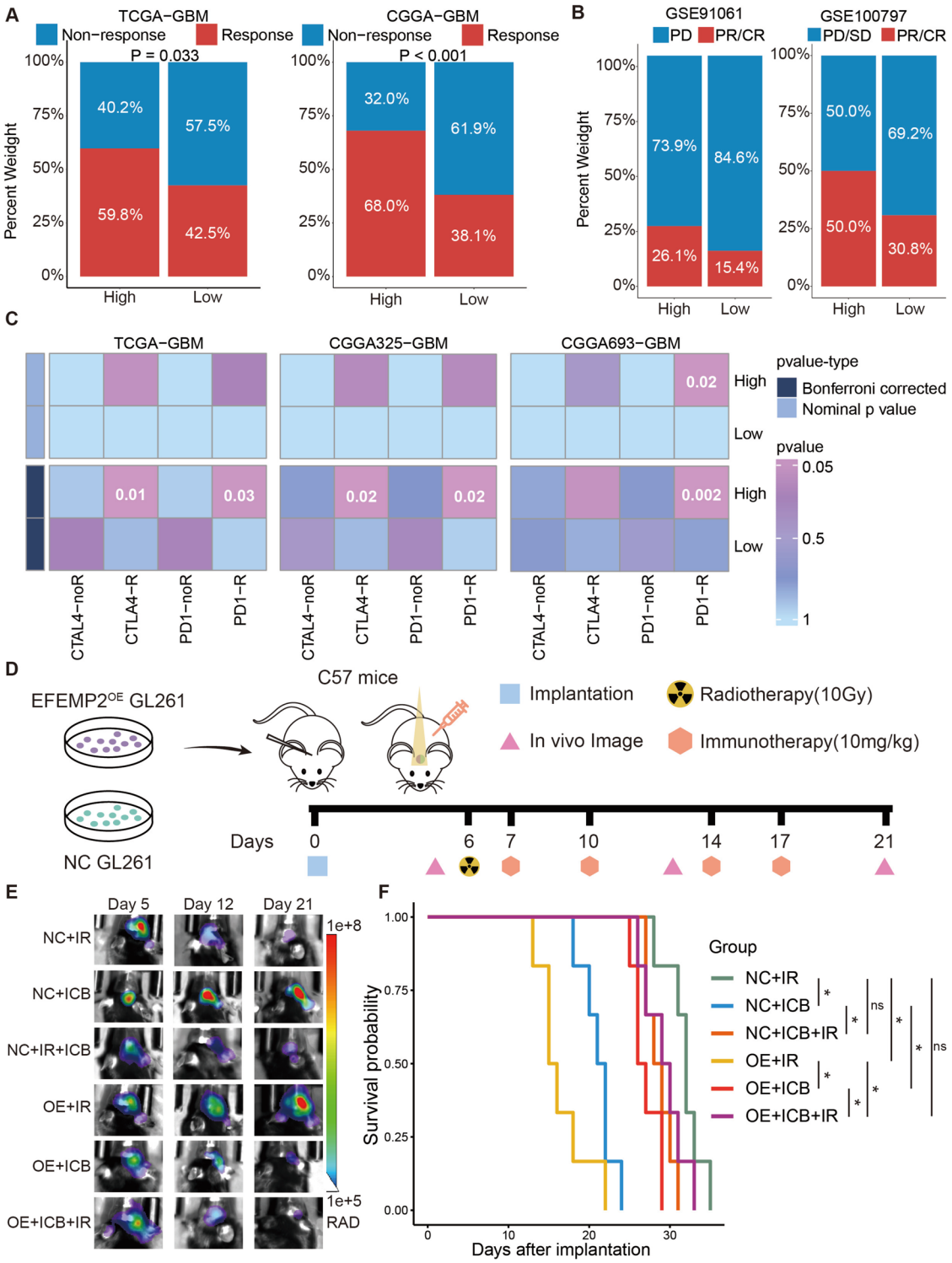


**Fig. 6** The association between DRS and immunotherapy response. **A** Differential proportions of the immunotherapy responders of the DRS groups in TCGA and CGGA cohorts predicted by the TIDE algorithm. **B** The Immunotherapy benefit rate of different DRS groups in GSE91061 and GSE100797 cohorts. **C** The potential response to immune checkpoint inhibitors of each DRS group estimated by submap algorithm. **D** Schematic illustration of combination irradiation with immune checkpoint blockade in EFEMP2$^{OE}$ and untreated C57BL6 mice. **E** Images of bioluminescence in mice during 21 days after intracranial injection of indicated GL261 cells. **F** Survival of C57BL6 mice bearing EFEMP2$^{OE}$ or untreated GL261 under different treatments (log-rank test, n = 6). *PD* progressive disease, *SD* stable disease, *PR* partial response, *CR* complete response, *IR* irradiation, *ICB* immune checkpoint blockade

observed that tumor antigen presentation and infiltration of immune cells were greater in GBM patients with high DRSs than in those with low DRSs, which provided better conditions for antitumor immunity after ICB treatment. Also, GL261-bearing mouse models with overexpressing EFEMP2 could benefit from ICB, whereas untreated GBM bearing mice were resistant to this regimen. A previous study reported that EFEMP2 upregulated PD-L1 expression in ovarian cancer cells, which may explain the relationship between EFEMP2 expression and the immunotherapy response. Therefore, it is not currently feasible to apply immunotherapy universally in GBM and DRS could serve as a quantitative tool to identify immunotherapeutic efficacy.

The combination of radiotherapy and immunotherapy has always been a promising strategy as well as a formidable challenge for treating GBM. Although the combined strategy has been validated in other cancers, it is difficult to replicate this success in GBM. Notably, the combination of immunotherapy and radiotherapy had synergistic therapeutic efficacy on EFEMP2$^{OE}$ GBM instead of untreated GBM in a tumor-bearing mouse model. A previous study illustrated that infiltration of T cells was positively correlated with the radiotherapy response, indicating that T cells mediate the local cytotoxic effects of radiotherapy (Yost et al. 2019; Arina et al. 2020). The application of ICB can amplify T-cell-mediated elimination (Sun et al. 2018). The synergistic effect of immunoradiotherapy was observed only in high DRS GBM, which is likely due to the relatively high infiltration of immune cells at baseline. Consequently, for GBM patients with high DRS or EFEMEP2 expression, immunotherapy should be combined with radiotherapy to achieve better clinical advantages.

Despite the results presented above, there are limitations in this study indubitably. Further studies are needed to validate the prognostic and therapeutic value of the DRS in clinical trials. Delving into the mechanisms by which high expression of EFEMP2 causes different therapeutic responses and TME remodeling is crucial for future clinical applications.

In conclusion, we comprehensively assessed DRGs in GBM and established that the DRS was correlated with reduced survival time, hampered tumor immunity, radioresistance and immunotherapeutic response, identifying EFEMP2 as the core gene. For radioresistant GBM patients with high DRS or EFEMP2 expression, the combination of radiotherapy and immunotherapy may be a viable treatment option. These findings contribute to optimizing the clinical management of GBM and offer a novel strategy for immunotherapy applications.

## Conclusions

Our study established a disulfidptosis-related signature that is a effective predictor in evaluating the prognosis and radiosensitivity of GBM. We explored the role of EFEMP2 in promoting the radioresistance of GBM and its impact on immunotherapy response, which provide a robust foundation for anti-tumor therapy.

**Supplementary Information** The online version contains supplementary material available at https://doi.org/10.1007/s00432-025-06159-0.

**Author contributions** Chen Chen: conceptualization, formal analysis, data curation, methodology, resources, validation, visualization, writing—original draft; Peixin Tan: investigation, visualization, writing—original draft; Wenqing Feng: formal analysis, validation; Yuan Lei: funding acquisition, writing—review & editing; Shushu Hu: formal analysis, validation; Dehuan Xie: writing—review & editing; Yantan Liu: writing—review & editing; Chen Ren: conceptualization, project administration, supervision; Shasha Du: conceptualization, project administration, funding acquisition, surpervision. Chen Chen and Peixin Tan contributed equally to this study.

**Funding** The present study was funded by the National Natural Science Foundation of China (Grant No. 82172671 and No.82202855), the Science and Technology Projects in Guangzhou (Grant No.2023A04J0518) and the High-level Hospital Construction Project of Guangdong Provincial People's Hospital (Grant No.KY012022119).

**Availability of data and materials** The public datasets analysed during the current study are available in the Gliovis (http://gliovis.bioinfo.cnio.es/), UCSC Xena (https://xena.ucsc.edu/), TCGA (https://www.cancer.gov/ccg/research/genome-sequencing/tcga), CGGA (http://www.cgga.org.cn/), GEO (https://www.ncbi.nlm.nih.gov/geo/) and TISICH (http://tisch.comp-genomics.org/home/) databases (Bowman et al. 2016; Goldman et al. 2020; Zhao et al. 2021; Lauss et al. 2017; Riaz et al. 2017; Neftel et al. 2019). Accession codes were provided in method section.

## Declarations

**Conflict of interest** The authors declare no competing interests.

**Ethical approval and consent to participate** All animal experiments were approved by the Animal Ethics Committee of Guangdong Provincial Peoples Hospital, Southern Medical University, China (Approval No. KY2023-001-01) and conducted in accordance with the Guidelines for Care and Use of Laboratory Animals at Southern Medical University, and all patients signed informed consent.

**Consent for publication** Not applicable.

## References


Aktar N et al (2022) Understanding of immune escape mechanisms and advances in cancer immunotherapy. J Oncol 2022:8901326. https://doi.org/10.1155/2022/8901326

Arina A, Gutiontov SI, Weichselbaum RR (2020) Radiotherapy and immunotherapy for cancer: from "Systemic" to "Multisite." Clin Cancer Res 26:2777–2782. https://doi.org/10.1158/1078-0432.Ccr-19-2034

Bao S et al (2006) Glioma stem cells promote radioresistance by preferential activation of the DNA damage response. Nature 444:756–760. https://doi.org/10.1038/nature05236

Bowman RL, Wang Q, Carro A, Verhaak RGW, Squatrito M (2016) GlioVis data portal for visualization and analysis of brain tumor expression datasets. Neuro Oncol 19:139–141. https://doi.org/10.1093/neuonc/now247

Chen H, Yang W, Li Y, Ma L, Ji Z (2023) Leveraging a disulfidptosis-based signature to improve the survival and drug sensitivity of bladder cancer patients. Front Immunol 14:1198878. https://doi.org/10.3389/fimmu.2023.1198878

Deng L et al (2014) Irradiation and anti-PD-L1 treatment synergistically promote antitumor immunity in mice. J Clin Invest 124:687–695. https://doi.org/10.1172/jci67313

Eschrich SA et al (2009) A gene expression model of intrinsic tumor radiosensitivity: prediction of response and prognosis after chemoradiation. Int J Radiat Oncol Biol Phys 75:489–496. https://doi.org/10.1016/j.ijrobp.2009.06.014

Fan W et al (2022) A novel chemokine-based signature for prediction of prognosis and therapeutic response in glioma. CNS Neurosci Ther 28:2090–2103. https://doi.org/10.1111/cns.13944

Fu J et al (2020) Large-scale public data reuse to model immunotherapy response and resistance. Genome Med 12:21. https://doi.org/10.1186/s13073-020-0721-z

Goldman MJ et al (2020) Visualizing and interpreting cancer genomics data via the Xena platform. Nat Biotechnol 38:675–678. https://doi.org/10.1038/s41587-020-0546-8

Grimes DR (2022) Limitations of the radiosensitivity index as a direct prognostic marker. Lancet Oncol 23:1352–1353. https://doi.org/10.1016/s1470-2045(22)00553-8

Hoshida Y (2010) Nearest template prediction: a single-sample-based flexible class prediction with confidence assessment. PLoS ONE 5:e15543. https://doi.org/10.1371/journal.pone.0015543

Hoshida Y, Brunet JP, Tamayo P, Golub TR, Mesirov JP (2007) Subclass mapping: identifying common subtypes in independent disease data sets. PLoS ONE 2:e1195. https://doi.org/10.1371/journal.pone.0001195

Hu C et al (2022) Cell marker 2.0: an updated database of manually curated cell markers in human/mouse and web tools based on scRNA-seq data. Nucleic Acids Res 51:D870–D876. https://doi.org/10.1093/nar/gkac947

Huang L et al (2020) EFEMP2 indicates assembly of M0 macrophage and more malignant phenotypes of glioma. Aging (Albany NY) 12:8397–8412. https://doi.org/10.18632/aging.103147

Iser IC, Pereira MB, Lenz G, Wink MR (2017) The epithelial-to-mesenchymal transition-like process in glioblastoma: an updated systematic review and in silico investigation. Med Res Rev 37:271–313. https://doi.org/10.1002/med.21408

Johannessen TC et al (2013) The DNA repair protein ALKBH2 mediates temozolomide resistance in human glioblastoma cells. Neuro Oncol 15:269–278. https://doi.org/10.1093/neuonc/nos301

Kang N, Zhou J, Xu J, Zhou D, Shi W (2019) EFEMP2 inhibits breast cancer invasion and metastasis in vitro and in vivo. Onco Targets Ther 12:8915–8933. https://doi.org/10.2147/ott.S221219

Kim JE et al (2017) Combination therapy with anti-PD-1, Anti-TIM-3, and focal radiation results in regression of murine gliomas. Clin Cancer Res 23:124–136. https://doi.org/10.1158/1078-0432.Ccr-15-1535

Lang X et al (2019) Radiotherapy and immunotherapy promote tumoral lipid oxidation and ferroptosis via synergistic repression of SLC7A11. Cancer Discov 9:1673–1685. https://doi.org/10.1158/2159-8290.Cd-19-0338

Langfelder P, Horvath S (2008) WGCNA: an R package for weighted correlation network analysis. BMC Bioinformatics 9:559. https://doi.org/10.1186/1471-2105-9-559

Lauss M et al (2017) Mutational and putative neoantigen load predict clinical benefit of adoptive T cell therapy in melanoma. Nat Commun 8:1738. https://doi.org/10.1038/s41467-017-01460-0

Leek JT, Johnson WE, Parker HS, Jaffe AE, Storey JD (2012) The sva package for removing batch effects and other unwanted variation in high-throughput experiments. Bioinformatics 28:882–883. https://doi.org/10.1093/bioinformatics/bts034

Li N, Ji GX, Yang ZY (2022) EFEMP2 increases the invasion ability of cervical cancer cells by promoting EMT via the Raf/MEK/ERK signaling pathway. Neoplasma 69:1185–1197. https://doi.org/10.4149/neo_2022_220117N74

Liberzon A et al (2015) The Molecular Signatures Database (MSigDB) hallmark gene set collection. Cell Syst 1:417–425. https://doi.org/10.1016/j.cels.2015.12.004

Lim M et al (2022) Phase III trial of chemoradiotherapy with temozolomide plus nivolumab or placebo for newly diagnosed glioblastoma with methylated MGMT promoter. Neuro Oncol 24:1935–1949. https://doi.org/10.1093/neuonc/noac116

Liu X et al (2023) Actin cytoskeleton vulnerability to disulfide stress mediates disulfidptosis. Nat Cell Biol 25:404–414. https://doi.org/10.1038/s41556-023-01091-2

Lu X et al (2019) Immune signature-based subtypes of cervical squamous cell carcinoma tightly associated with human papillomavirus type 16 expression, molecular features, and clinical outcome. Neoplasia 21:591–601. https://doi.org/10.1016/j.neo.2019.04.003

Neftel C et al (2019) An integrative model of cellular states, plasticity, and genetics for glioblastoma. Cell 178:835-849.e821. https://doi.org/10.1016/j.cell.2019.06.024

Pineda B et al (2019) Malignant glioma therapy by vaccination with irradiated C6 cell-derived microvesicles promotes an antitumoral immune response. Mol Ther 27:1612–1620. https://doi.org/10.1016/j.ymthe.2019.05.016

Rajendran S et al (2023) Single-cell RNA sequencing reveals immunosuppressive myeloid cell dive rsity during malignant progression in a murine model of glioma. Cell Rep 42:112197. https://doi.org/10.1016/j.celrep.2023.112197

Reardon DA et al (2020) Effect of Nivolumab vs Bevacizumab in Patients With Recurrent Glioblastoma: The CheckMate 143 Phase 3 Randomized Clinical Trial. JAMA Oncol 6:1003–1010. https://doi.org/10.1001/jamaoncol.2020.1024

Riaz N et al (2017) Tumor and microenvironment evolution during immunotherapy with nivolumab. Cell 171:934-949.e916. https://doi.org/10.1016/j.cell.2017.09.028

Sampson JH et al (2016) A randomized, phase 3, open-label study of nivolumab versus temozolomide (TMZ) in combination with radiotherapy (RT) in adult patients (pts) with newly diagnosed, O-6-methylguanine DNA methyltransferase (MGMT)-unmethylated glioblastoma (GBM): CheckMate-498. J Clin Oncol

34:TPS2079. https://doi.org/10.1200/JCO.2016.34.15_suppl.TPS2079
Shen X, Jin X, Fang S, Chen J (2023) EFEMP2 upregulates PD-L1 expression via EGFR/ERK1/2/c-Jun signaling to promote the invasion of ovarian cancer cells. Cell Mol Biol Lett 28:53. https://doi.org/10.1186/s11658-023-00471-8
Song L et al (2020) EFEMP2 suppresses the invasion of lung cancer cells by inhibiting epithelial-mesenchymal transition (EMT) and down-regulating MMPs. Onco Targets Ther 13:1375–1396. https://doi.org/10.2147/ott.S236111
Stupp R et al (2017) Effect of tumor-treating fields plus maintenance temozolomide vs maintenance temozolomide alone on survival in patients with glioblastoma: a randomized clinical trial. JAMA 318:2306–2316. https://doi.org/10.1001/jama.2017.18718
Sun G, Liu W (2024) The neutrophil extracellular traps-related gene signature predicts the prognosis of glioblastoma multiforme. Folia Neuropathol. https://doi.org/10.5114/fn.2023.132980
Sun S, Hao H, Yang G, Zhang Y, Fu Y (2018) Immunotherapy with CAR-modified T cells: toxicities and overcoming strategies. J Immunol Res 2018:2386187. https://doi.org/10.1155/2018/2386187
Sun D et al (2023) Classification of tumor immune microenvironment according to programmed death-ligand 1 expression and immune infiltration predicts response to immunotherapy plus chemotherapy in advanced patients with NSCLC. J Thorac Oncol 18:869–881. https://doi.org/10.1016/j.jtho.2023.03.012
Szklarczyk D et al (2019) STRING v11: protein-protein association networks with increased coverage, supporting functional discovery in genome-wide experimental datasets. Nucleic Acids Res 47:D607-d613. https://doi.org/10.1093/nar/gky1131
Szulzewsky F et al (2015) Glioma-associated microglia/macrophages display an expression profile different from M1 and M2 polarization and highly express Gpnmb and Spp 1. PLoS ONE 10:e0116644. https://doi.org/10.1371/journal.pone.0116644
Verhaak RG et al (2010) Integrated genomic analysis identifies clinically relevant subtypes of glioblastoma characterized by abnormalities in PDGFRA, IDH1, EGFR, and NF1. Cancer Cell 17:98–110. https://doi.org/10.1016/j.ccr.2009.12.020
Wang L et al (2015) EFEMP2 is upregulated in gliomas and promotes glioma cell proliferation and invasion. Int J Clin Exp Pathol 8:10385–10393
Wang Z, Zhang H, Xu S, Liu Z, Cheng Q (2021) The adaptive transition of glioblastoma stem cells and its implications on treatments. Signal Transduct Target Ther 6:124. https://doi.org/10.1038/s41392-021-00491-w
Wang T et al (2023a) Disulfidptosis classification of hepatocellular carcinoma reveals correlation with clinical prognosis and immune profile. Int Immunopharmacol 120:110368. https://doi.org/10.1016/j.intimp.2023.110368
Wang X, Yang J, Yang F, Mu K (2023b) The disulfidptosis-related signature predicts prognosis and immune features in glioma patients. Sci Rep 13:17988. https://doi.org/10.1038/s41598-023-45295-w
Wu CY et al (2014) Enhanced cancer radiotherapy through immunosuppressive stromal cell destruction in tumors. Clin Cancer Res 20:644–657. https://doi.org/10.1158/1078-0432.Ccr-13-1334
Xia Y, Jiang L, Zhong T (2018) The role of HIF-1α in chemo-/radioresistant tumors. Onco Targets Ther 11:3003–3011. https://doi.org/10.2147/ott.S158206
Yang X et al (2024) Integrated multiomic analysis reveals disulfidptosis subtypes in glioblastoma: implications for immunotherapy, targeted therapy, and chemotherapy. Front Immunol 15:1362543. https://doi.org/10.3389/fimmu.2024.1362543
Yin K, Xia X, Rui K, Wang T, Wang S (2020) Myeloid-derived suppressor cells: a new and pivotal player in colorectal cancer progression. Front Oncol 10:610104. https://doi.org/10.3389/fonc.2020.610104
Yost KE et al (2019) Clonal replacement of tumor-specific T cells following PD-1 blockade. Nat Med 25:1251–1259. https://doi.org/10.1038/s41591-019-0522-3
You G et al (2023) scRNA-seq and proteomics reveal the distinction of M2-like macrophages between primary and recurrent malignant glioma and its critical role in the recurrence. CNS Neurosci Ther. https://doi.org/10.1111/cns.14269
Yu P et al (2024) PRMT6-mediated transcriptional activation of ythdf2 promotes glioblastoma migration, invasion, and emt via the wnt-β-catenin pathway. J Exp Clin Cancer Res 43:116. https://doi.org/10.1186/s13046-024-03038-3
Zeiner PS et al (2019) Distribution and prognostic impact of microglia/macrophage subpopulations in gliomas. Brain Pathol 29:513–529. https://doi.org/10.1111/bpa.12690
Zeng J et al (2013) Anti-PD-1 blockade and stereotactic radiation produce long-term survival in mice with intracranial gliomas. Int J Radiat Oncol Biol Phys 86:343–349. https://doi.org/10.1016/j.ijrobp.2012.12.025
Zeng D et al (2021) IOBR: multi-omics immuno-oncology biological research to decode tumor microenvironment and signatures. Front Immunol 12:687975. https://doi.org/10.3389/fimmu.2021.687975
Zhang L et al (2018) Lineage tracking reveals dynamic relationships of T cells in colorectal cancer. Nature 564:268–272. https://doi.org/10.1038/s41586-018-0694-x
Zhang D et al (2022) STEAP2 promotes osteosarcoma progression by inducing epithelial-mesenchymal transition via the PI3K/AKT/mTOR signaling pathway and is regulated by EFEMP2. Cancer Biol Ther 23:1–16. https://doi.org/10.1080/15384047.2022.2136465
Zhang B, Xie L, Liu J, Liu A, He M (2023) Construction and validation of a cuproptosis-related prognostic model for glioblastoma. Front Immunol 14:1082974. https://doi.org/10.3389/fimmu.2023.1082974
Zhang M et al (2023) A novel cuproptosis-related gene signature to predict prognosis in Glioma. BMC Cancer 23:237. https://doi.org/10.1186/s12885-023-10714-8
Zhang W et al (2024) Pan-cancer evaluation of regulated cell death to predict overall survival and immune checkpoint inhibitor response. Npj Precis Oncol 8:77. https://doi.org/10.1038/s41698-024-00570-5
Zhao Z et al (2021) Chinese glioma genome atlas (CGGA): a comprehensive resource with functional genomic data from Chinese glioma patients. Genomics Proteomics Bioinformatics 19:1–12. https://doi.org/10.1016/j.gpb.2020.10.005
Zhou Q et al (2019) EFEMP2 suppresses epithelial-mesenchymal transition via Wnt/β-catenin signaling pathway in human bladder cancer. Int J Biol Sci 15:2139–2155. https://doi.org/10.7150/ijbs.35541
Zhou Y et al (2024) Cross-talk between disulfidptosis and immune check point genes defines the tumor microenvironment for the prediction of prognosis and immunotherapies in glioblastoma. Sci Rep 14:3901. https://doi.org/10.1038/s41598-024-52128-x